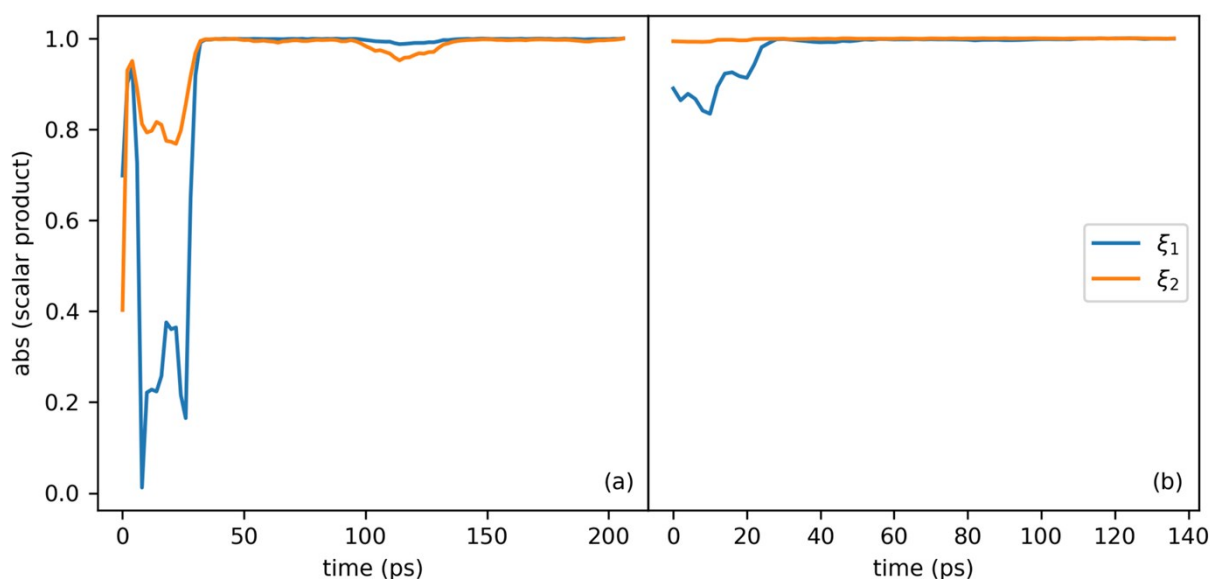


# Supporting Materials

## S1 Harmonic Linear Discriminant analysis

The convergence of HLDA coefficients was tested monitoring in time the absolute value of the scalar product between the instantaneous value of each CV and its final one.



**Figure S1.** Converged behavior of HLDA CVs,  $\xi_1$  and  $\xi_2$ , (a) for **1a + 1b** reaction and (b) for **2a + 2b**.

		$d_1$	$d_2$	$d_3$	$d_4$	$d_5$	$d_6$	$d_7$
<b>1a + 1b</b>	$\xi_1$	- 0.353	- 0.388	0.581	0.573	- 0.223	- 0.059	- 0.078
	$\xi_2$	- 0.579	- 0.582	0.295	0.239	0.399	0.109	0.108
<b>2a + 2b</b>	$\xi_1$	0.327	0.340	0.280	0.319	- 0.717	- 0.193	- 0.215
	$\xi_2$	- 0.491	- 0.498	0.514	0.494	- 0.040	- 0.028	- 0.026

**Table S1.**  $\xi_1$  and  $\xi_2$  are linear combinations of  $d_{1-7}$ , in this table their coefficients are reported.

Because of the discrimination properties of HLDA, it is already possible to have an insight into the reaction looking at the differences of the signs in Table S1.  $\xi_1$  and  $\xi_2$  identify a projection in  $d_{1-7}$  descriptor subspace, so their global sign does not have a *per-se* meaning. On the other hand, a particular CV well describes a process that implies the elongation of all the distances with coefficients of a given sign and the contraction of all the distances with coefficients of the opposite sign. Thus, this CV is a good identifier between the starting and final states of this process. For example for **2a + 2b**,  $\xi_1$  distinguishes well between reactants and products, while  $\xi_2$  between the two products. Moreover, from sign accordance it is possible to see

that in all the reaction of interest  $d_1$  and  $d_2$  elongate or contract together, as well as for  $d_3$  and  $d_4$  couple and for  $d_5$ ,  $d_6$  and  $d_7$ .

## S2 Error Assessment and Convergence Control of the Free Energy Differences between Reactants and Products.

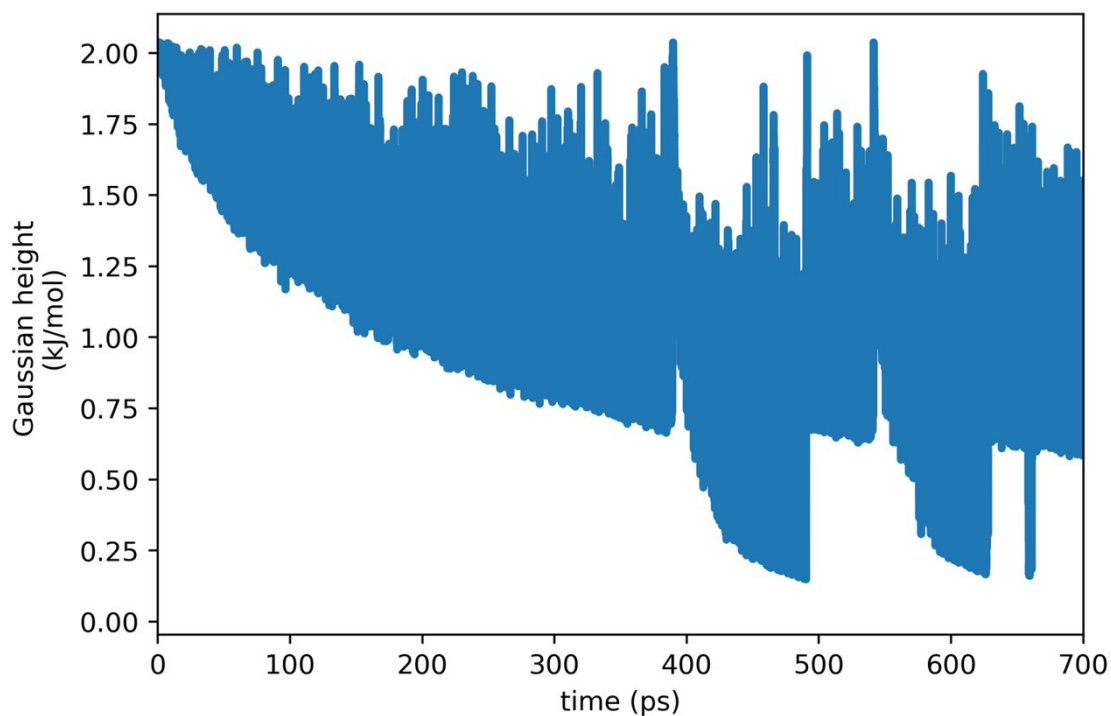


**Figure S2.** Gaussians height as function of time. At the start of the simulation, the system is visiting the reactants basin and the height is exponentially decreased. When it moves towards the first product (at  $t=380$  ps), the height of the Gaussians reaches again the starting value of 2, and then it decreases faster, being this area narrower than the reactants one. When it goes back into reactants basins ( $t=500$  ps), height turns again to the value it had at  $t=380$  and keeps on decreasing. As in the previous case, visiting the second product (from  $t=550$  ps), height first assumes values of 2 and then rapidly decrease.

	<b>1a + 1b</b>	<b>2a + 2b</b>
$\tau$	$5 \cdot 10^{-2}$	$5 \cdot 10^{-2}$
$h_0$	0.02	0.01
$\gamma$	55	60
$\sigma_0$	$9.6 \cdot 10^{-2}$	$2.6 \cdot 10^{-1}$

t	$5 \cdot 10^3$	$5 \cdot 10^3$
---	----------------	----------------

**Table S2.** Parameter for the adaptive-variance WT-MetaD simulations.  $\tau$  is the Gaussian deposition rate and  $t$  the simulation time (ps).  $h_0$  is the initial Gaussian height and  $\sigma_0$  its initial standard deviation (kJ/mol).  $\gamma$  is the bias factor.

We controlled the convergence of the WT-metaD runs monitoring in time the free energy ( $F$ ) differences between the basins (Figure S3), computed according to:

$$F_{basin} = -k_B T \ln \left( \int_{basin} d\xi_1 d\xi_2 e^{-\frac{F(\xi_1, \xi_2)}{k_B T}} \right), \#(S1)$$

with  $k_B$  the Boltzmann constant,  $T$  the temperature. After  $t=7$  ns, it starts fluctuating around a converged value.

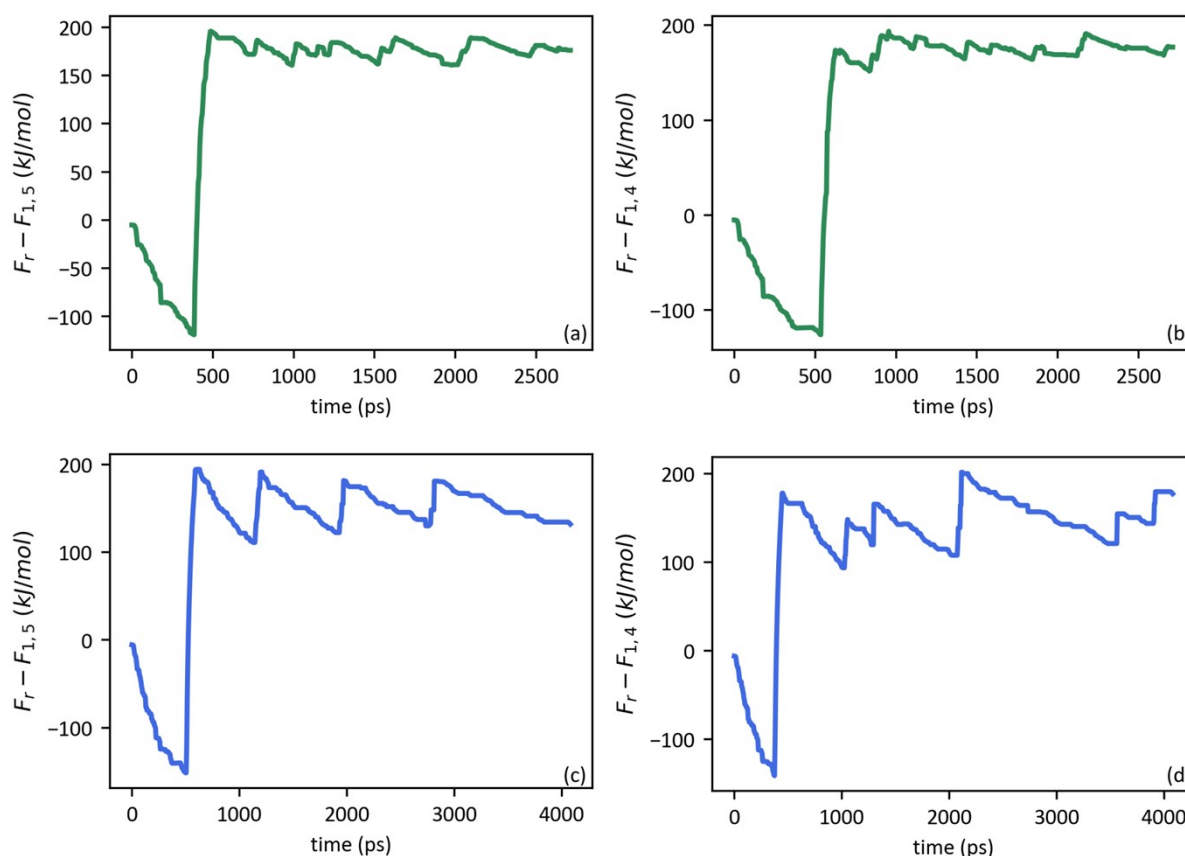


**Figure S3.** Differences in free energy of the basins in time. Upper panels: **1a + 1b** reaction, lower panel: **2a + 2b** reaction

The final estimation of the free energy differences is associated to a statistical error, using block average on the converged data (from 0.7 ns to 3 ns).<sup>1</sup>

### S3 Transition State Ensembles Characterization

In order to discriminate between the ensembles of Figure 5 of the manuscript, an additional CV is needed, which we name  $\xi_3$ . For 1,4 triazole  $\xi_3=d_1-d_2$ , while for 1,5 triazole  $\xi_3=d_3-d_4$ . To get the unbiased probability the FES (function of  $\xi_1$  and  $\xi_2$ ) was reweighted on  $\xi_1$ ,  $\xi_2$  and  $\xi_3$  and the associate free energy was calculated using Eq. (S1). Finally, the probability was obtained according to:

$$p = e^{-F/k_B T}.$$

### S4 Restraint Geometry Optimization for 2a + 2b

Likewise the **1a + 1b** case the results are commented again in light of the restraint geometry optimizations (Figure S4). The resulting PES preserve the features of the **1a + 1b** ones. As a consequence, the geometries found in  $\mathbf{t}_{1,4}$  and  $\mathbf{t}_{1,5}$  regions show strong analogies to **1a + 1b** system, with the exception of  $\mathbf{t}_{1,5}^c$  case, that is not found for **2a + 2b** system. This absence can be explained if we consider that there is an additional effect of increased steric hindrance due of the increased size of the substituents. The latter is responsible also for the inversion in probability of the concerted ( $\mathbf{t}_{1,4}^c$ ) and the stepwise states ( $\mathbf{t}_{1,4}^{s1}$ ) towards 1,4 triazole.

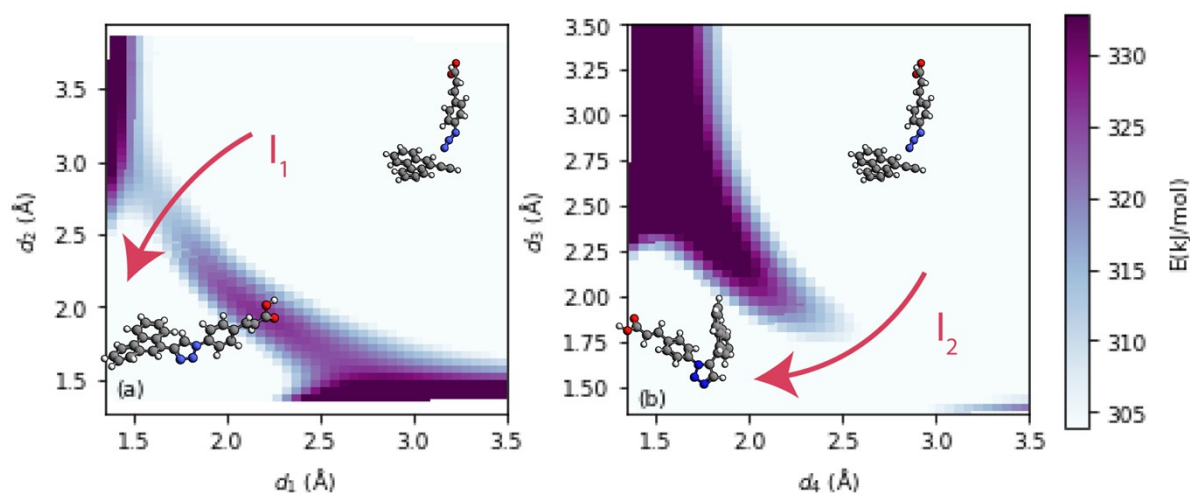


**Figure S4.** Energy grid obtained with restraint geometry optimizations for **2a + 2b** reaction.

### S5 Dispersion corrections to WT-MetaD

For the system **1a + 1b**, we repeated WT-MetaD calculations including the Grimme's D3 dispersion corrections (PM6-D3).<sup>2,3</sup> Quantitative analysis (Table S3) does not bring any significant difference in terms of reaction heat, being the products free energies compatible within the statistical error. It is

worth stressing that the associated statistical error is obtained with the block average analysis, which represents a lower limit for the actual error. Therefore, the small differences between the two levels of theory in the overall energetics are of minor relevance.

	$\Delta E$ PM6	$\Delta F$ PM6	$\Delta E$ PM6 D3	$\Delta F$ PM6-D3
1,4 triazole	-222	$-176 \pm 2$	-227	$-205 \pm 13$
1,5 triazole	-224	$-180 \pm 10$	-230	$-189 \pm 9$

**Table S3** Differences in energy and free energy (kJ/mol) between the metastable states obtained with WT-MetaD at PM6 and PM6-D3 levels for **1a** + **1b** reaction. Reactants are set as reference.

Concerning the FES shape, one can observe that at PM6-D3 level the FES (Figure S5) preserves the main features observed without the dispersion corrections (Figure 4(a) of the manuscript). The lateral corridors are populated by the same geometries observed at PM6 levels.

The most relevant differences are given by the absence of a local free energy minima associated to the **t\*** intermediate and to a more broadened transition area. The small high energy area identified in the bottom part of  $p_{1,4}$  basin is associated to a geometry in which the 1,4 triazole central ring is bent and extremely distorted, and therefore is not considered in the basins analysis.

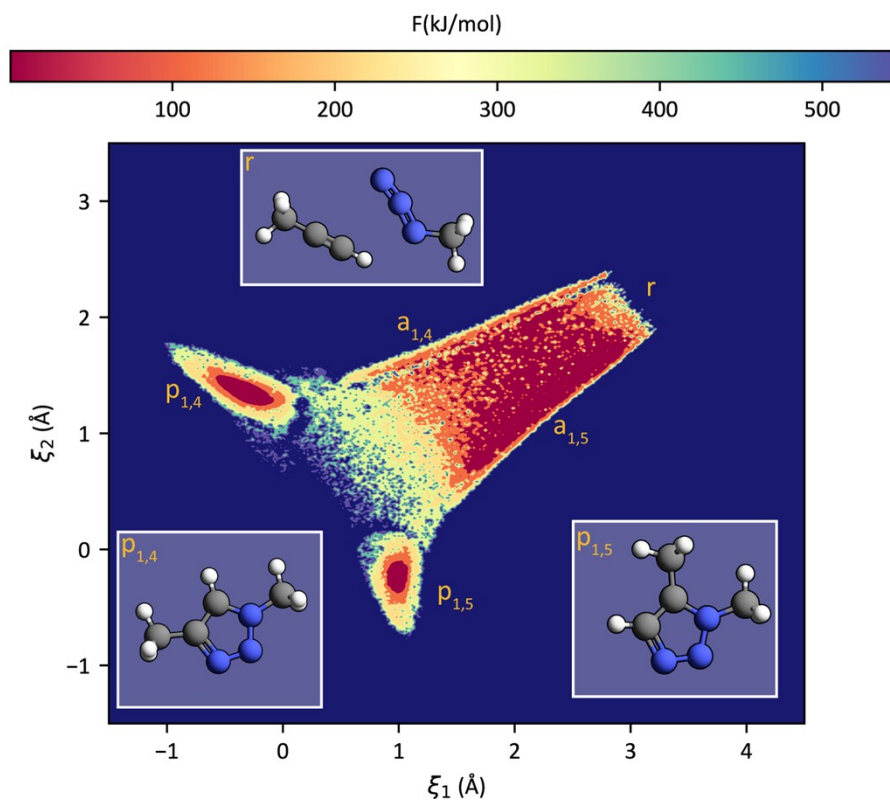


**Figure S5** PM6-D3 reweighted FES for **1a** + **1b** system. *r* label indicate the reactants,  $p_x$  (with  $x=1,4$  and  $1,5$ ) the products.

## S6 Dispersion corrections to VA

In the following, we report the vibrational analysis results at PME-D3 level (performed after geometry optimizations at the same level of theory). Table S4 shows the same trend found without the D3 correction.

	$\Delta E$		$\Delta F$ VA	
	1,4 triazole	1,5 triazole	1,4 triazole	1,5 triazole
<b>1a + 1b</b>	-227	-230	-231	-232
<b>2a + 2b</b>	-216	-229	-158	-170

**Table S4** Energetic of the reaction (kJ/mol) resulting from vibrational analysis with D3 dispersion correction. Reactants are set as reference.

## BIBLIOGRAPHY

- (1) Flyvbjerg, H.; Petersen, H. G. Error Estimates on Averages of Correlated Data. *The Journal of Chemical Physics* **1989**, *91* (1), 461–466. <https://doi.org/10.1063/1.457480>.
- (2) Grimme, S. Supramolecular Binding Thermodynamics by Dispersion-Corrected Density Functional Theory. *Chemistry – A European Journal* **2012**, *18* (32), 9955–9964. <https://doi.org/10.1002/chem.201200497>.
- (3) Řezáč, J.; Hobza, P. Advanced Corrections of Hydrogen Bonding and Dispersion for Semiempirical Quantum Mechanical Methods. *J. Chem. Theory Comput.* **2012**, *8* (1), 141–151. <https://doi.org/10.1021/ct200751e>.